J. Condensed Matter Nucl. Sci. 38 (2024) 269–286

Research Article

Anomalous Heat Burst Triggered by Input Power Perturbations observed in Ni-Based Nanostructured Thin Films with Hydrogen

Y. Iwamura, T. Itoh, and Jirohta Kasagi

Research Center for Electron Photon Science, Tohoku University, 982-0826 Japan

T. Itoh, T. Takahashi, S. Yamauchi, M. Saito, S. Murakami, and T. Hioki

CLEAN PLANET Inc., 105-0022 Japan

T. Hioki

Institutes of Innovation for Future Society, Nagoya University, 464-8603, Japan

Abstract

The authors developed an innovative method to induce anomalously large heat generation phenomena that cannot be explained by known chemical processes. Ni-based nano-sized multilayer film is preloaded with hydrogen gas and heated rapidly to diffuse hydrogen and trigger the heat generation reaction. Two nano-sized metal multilayer composite samples, which were composed of Ni, Cu, and the other thin films on bulk Ni (25 mm × 25 mm × 0.1 mm), were used. Anomalous heat generations were observed during the experiments under vacuum condition ($<10^{-4}$ Pa) using nano-sized metal multilayer composites on Ni substrate, with hydrogen gas. Released energy evaluated with total amount of absorbed hydrogen reached to more than 10 keV/H. In addition to steady-state anomalous heat generation, spontaneous heat burst phenomena were sometimes observed. Based on the observation of spontaneous heat bursts, we can now trigger intentional heat bursts. The energy from even a single heat burst exceeds the energy produced by any known chemical reactions. Observation of heat bursts has improved the reliability of excess heat experiments. Samples that generated excess heat or heat bursts often show some areas of very high oxygen concentration after the experiment according to SEM-EDX and TOF-SIMS analyses.
 ISSN 2227-3123

Keywords: Anomalous heat, Heat burst, Excess heat, Nickel, Copper, Multilayer thin film, Nano-sized metal composite, Nano material, Hydrogen gas, Gas loading

1. Introduction

The authors have been studying energy generation using nano-sized multilayer metal composites with hydrogen gas. First, we briefly describe how we got started with our current research methodology. Originally, we discovered

 ISSN 2227-3123

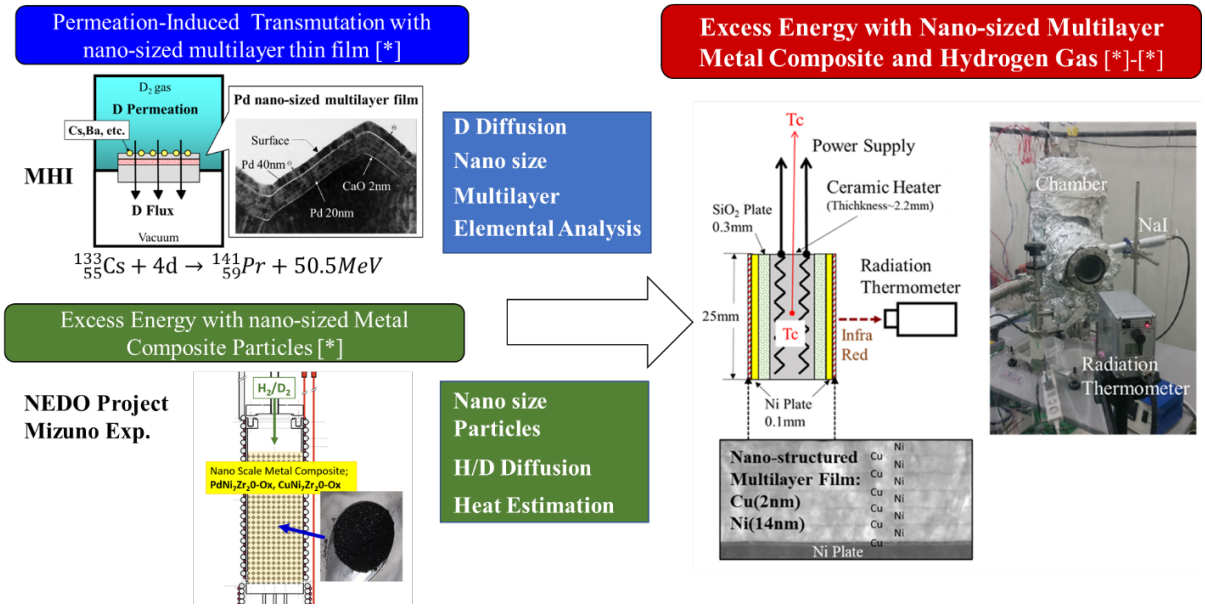

Figure 1. Background and Motivation of the Present Experimental Method.

transmutation phenomena induced by deuterium gas permeation through nanosized Pd multilayers doped with Cs and other elements [1]–[4]. We observed the transmutation of Cs into Pr by this method, which has been reproduced by other independent research institutes [5]. This study shows that the diffusion of deuterium and nano-sized multilayers are key factors in inducing the transmutation reaction [2], [4]. After moving to Tohoku University, we had a chance to participate in a national project funded by NEDO (New Energy and Industrial Technology Development Organization) to observe anomalous heat generation by deuterium or hydrogen absorption in Pd or Ni nanoparticles. We learned that anomalous phenomena occur not only with deuterium but also with light hydrogen, and that the nano-sized composite particle is one of the key factors to inducing the anomalous phenomena [6]–[8]. By combining the two methods, we have developed a new kind of experimental procedure to induce an exothermic reaction by loading light hydrogen in a nickel-based composite material with nano-sized multilayers, and then diffusing the light hydrogen through the nano-multilayers by rapid heating. This new experimental method is being used to elucidate the mechanism of the phenomenon. In addition, this method has led to a larger excess energy per hydrogen atom [9]–[16].

At present, the mechanism of this anomalous heat generation is not clearly understood. Based on observations of anomalous heating that cannot be explained by chemical reactions and nuclear transmutations, we speculate that the phenomenon may be of nuclear origin. However, since the mechanism has not yet been clearly elucidated, we have decided to call this phenomenon QHE (Quantum Hydrogen Energy) [9]. One of the reasons for this is that “nuclear” term is associated with a complicated and dangerous image that is difficult for the general public to accept. QHE can be defined as “An exothermic reaction induced by quantum phenomena during the diffusion process in a nanoscale metal composite material with hydrogen” shown in Fig. 2. The characteristics of QHE are as follows: 1) No CO_2 emission, and more than 10,000 times higher output energy than the combustion reaction of the same amount of hydrogen; 2) QHE does not emit harmful levels of radiation to the human body and has the potential to become a compact,

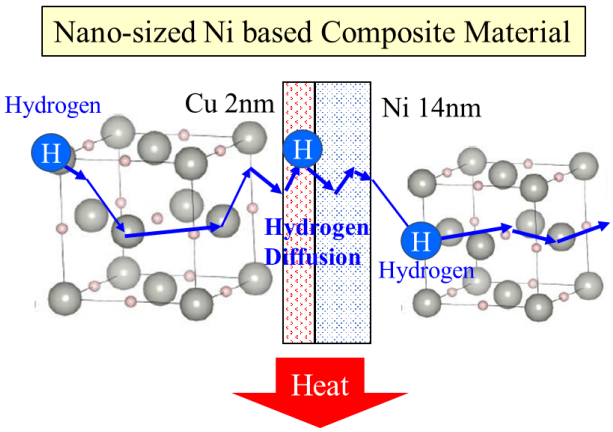

Figure 2. Quantum Hydrogen Energy (QHE)

high-power, CO_2-free energy source; 3) QHE could be used as an energy source for the production of electricity and heat.

2. Experimental

A schematic of our experimental apparatus is shown in Fig. 3(a). It is basically the same as in [9]–[10]. Two nano-sized metal multilayer composite samples, which were composed of Ni, Cu, CaO thin films on bulk Ni (25 mm $\times$ 25 mm $\times$ 0.1 mm), were placed in the center of the chamber. H_2 gas and its pressure were monitored by a Pirani gauge and a cold cathode gauge. The chamber was evacuated by a turbo molecular pump. The multilayer samples were heated up by a ceramic heater (MS-1000R; Sakaguchi E. H Voc Corp.) in which a thermocouple (TC; Pt-PtRh13%) was embedded. Surface temperatures for the two nano-sized metal multilayer composite samples were measured by two thermometers. They were made of InGaAs and dual wavelength mode, 1.55 μm and 1.35 μm, were usually used. During the surface temperature measurement, it was possible to measure the emissivity of the sample surface by switching between single wavelength mode and dual wavelength mode. Heater input power was supplied by a DC power source in constant voltage mode. The input voltage and current were measured both by voltage and current monitors provided by the power supply and an independent voltmeter and ammeter, respectively. Input power is calibrated using the voltmeter and the ammeter readings. Gamma-rays and neutrons were monitored by a NaI (Tl) scintillation counter (TCS-1172; Hitachi, Ltd.) and He-3 counter (TPS-1451; Hitachi Ltd.) during all experiments for safety reasons.

A detailed drawing of the Ni based nano-sized metal multilayer composite is shown in Fig. 3(b). It was composed of a Ni Plate (25 mm square and 0.1 mm thick) and Cu-Ni multilayer thin film (20 mm diameter circle and about 100 nm thick). These samples were fabricated by the magnetron sputtering or Ar ion beam method. The top layer of the sample is always Ni. Two nano-sized metal multilayer composite samples were heated by the ceramic heater (25 mm square and 2.2 mm thick) through SiO_2 plates (0.3 mm thick). If certain energy generation reactions occur on the surface of the samples, the temperature of the embedded thermocouple will rise. Simultaneously, infrared emission detected by the radiation thermometer, which corresponds to the surface temperature of the sample, would increase. Photos of the experimental set-ups and STEM image of Cu-Ni multilayer thin film are shown in Fig. 3.

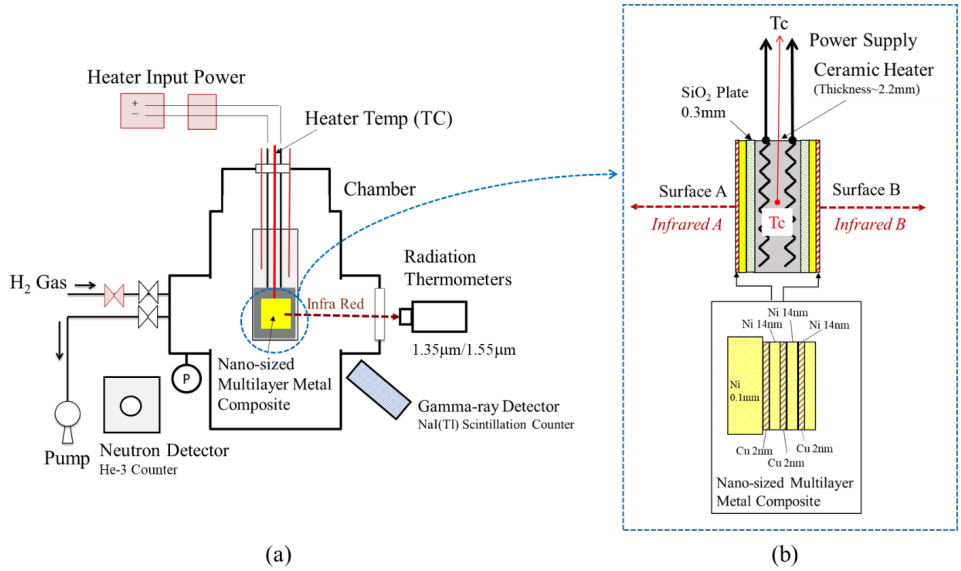

Figure 3. Experimental set-up; (a) Schematic of experimental apparatus, (b) Detail drawing around nano-sized multilayer metal composite.

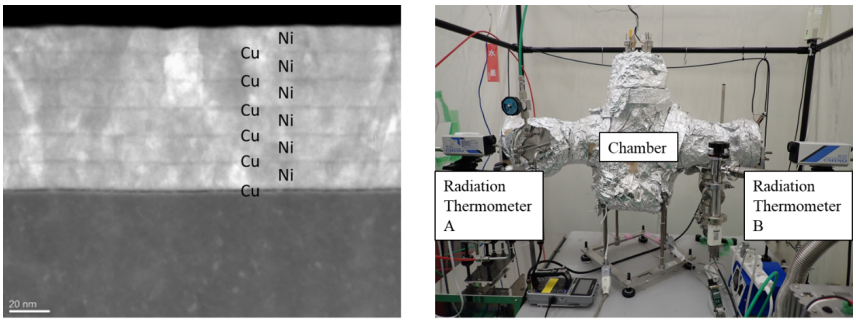

Figure 4. Photos of experimental apparatus and cross-sectional view of nano-sized metal multilayer composites; (a) STEM (Scanning transmission electron microscope) image of Cu-Ni multilayer thin film, (b) Outer view of the present experimental Set-up.

The experimental procedure is as follows. Two nano-sized metal multilayer composites were placed in the chamber and baked for 2-3 days at heater temperature 900°C to remove H_2O and other hydrocarbons from the surface under vacuum conditions.

According to general knowledge, Cu and Ni diffuse into each other during the baking process, forming a Cu-Ni alloy. However, in our multilayer film, Cu and Ni are not simply alloyed, especially when CaO, Y_2O_3, etc. are added to Ni. At present, we assume that this is due to the effect of oxygen formed on the surface during sputtering.

After the baking process, H_2 gas was introduced into the chamber up to about 200 Pa at 250°C. To change the hydrogen loading conditions, the pressure of H_2 gas was sometimes increased up to 30 kPa. H_2 gas was loaded for

about 16 hours. Then, H_2 gas was evacuated by the turbo molecular pump and simultaneously the samples were heated up by the ceramic heater up to 500∼900°C. These processes trigger heat generation reactions and anomalous heat. Typically, after 8 hours, the heater input was turned down and the samples were cooled down to 250°C. These processes (H_2 loading, heating up and cooling down samples) were repeated several times, with different heating temperatures or H_2 loading pressure.

During the above experimental procedure, hydrogen atoms are assumed to diffuse from the Ni plate through the nano-sized metal multilayer to the surface. The diffusion mechanism of hydrogen atoms is well known as "quantum diffusion" [17], although quantum diffusion is noticeable at temperatures much lower than the temperatures covered in this experiment. Hydrogen atoms are hopping from one site to another site in the metal. It is assumed that hydrogen flux is one of the key factors to induce the anomalous heat generation phenomena in the present experiments.

3. Results and Discussion

3.1. Excess Heat Evaluation

Excess Heat is evaluated based on the model described in Fig. 5(a) and the following equation (1).

$$k_{\mathrm{eff}}\frac{T_C - T_W}{L_{\mathrm{eff}}}A_{\mathrm{eff}} + A_S\sigma\left\{\varepsilon_A\left(T_{\mathrm{SA}}^4 - T_W^4\right) + \varepsilon_B\left(T_{\mathrm{SB}}^4 - T_W^4\right)\right\} + A_{\mathrm{Rloss}}\varepsilon_{\mathrm{Rloss}}\sigma\left(T_{\mathrm{Rloss}}^4 - T_W^4\right) = P_{\mathrm{in}} + H_{\mathrm{ex}}, \quad (1)$$

where k_{eff} is equivalent thermal conductivity, T_c is the thermocouple temperature embedded in the ceramic heater, T_w is the wall temperature of the chamber, L_{eff} and A_{eff} are effective length and effective surface area between the sample holder and wall, respectively. A_s is the surface area of the sample, T_S is the surface temperature, ε is the emissivity of the sample, σ is the Stefan–Boltzmann constant. subscript A and B means surface A and B, respectively. A_{Rloss}, ε_{Rloss} and T_{Rloss} are effective surface area; effective emissivity and effective surface temperature for radiation loss except from the sample surface, which is mainly derived from the sample holder. P_{in} is the electrical heater input and H_{ex} is excess power. This equation is obtained under the following assumptions.

1) Thermal conduction via H_2 gas is negligible because H_2 pressure is low.
2) Radiation from the chamber wall is negligible because T_w is room temperature.
3) The electrical input power is constant.

A blank run, in which same sized Ni bulk samples without multilayer thin films were used, was performed with the same procedure described above. Figure 5(b) shows the relationship between input power given to the ceramic heater and heater temperature detected by the thermocouple. As the radiation loss term from the sample holder is the same for Ni bulk and multilayer samples for the same temperature, generated excess heat power is evaluated based on the blank run result as shown in Fig. 3(b). Equation (1) for Ni bulk (subscript "0") is written as:

$$k_{\mathrm{eff}}\frac{T_{C0} - T_W}{L_{\mathrm{eff}}}A_{\mathrm{eff}} + A_S\sigma\left\{\varepsilon_{A0}\left(T_{SA0}^4 - T_W^4\right) + \varepsilon_{B0}\left(T_{SB0}^4 - T_W^4\right)\right\} + A_{\mathrm{Rloss}}\varepsilon_{\mathrm{Rloss}}\sigma\left(T_{Rloss0}^4 - T_W^4\right) = P_{\mathrm{in}}. \quad (2)$$

In the papers [9]–[10], excess heat analysis was done based on the assumption that ε is constant for Ni based nano-sized metal multilayer composite and Ni bulk. Emissivity ε can be measured by switching between two wavelengths mode and single wavelength mode. Actual measured emissivity was in the range of 0.1–0.2 at surface temperature 700–750°C, depending on the condition of the sample such as oxidation of surface or surface roughness, the vacuum of the experimental apparatus. However, the difference in emissivity between Ni bulk and Ni multilayer composite

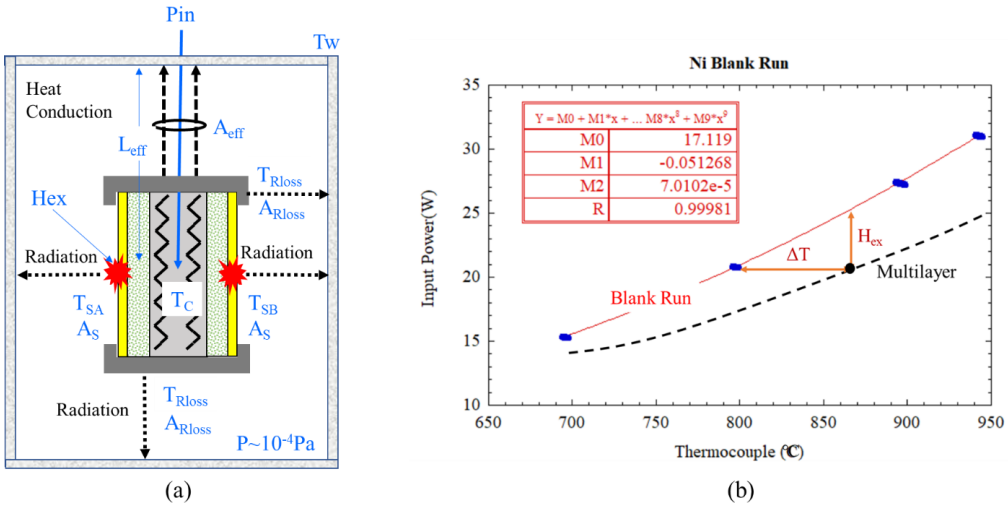

Figure 5. Excess heat evaluation; (a) Model of excess heat evaluation, (b) Relationship between input power (W) and thermocouple temperature (°C) for a blank run and a multilayer run.

samples is within 0.05, and the assumed condition is satisfied. Emissivity can be considered almost the same for the Ni bulk and multilayer composite samples.

Excess heat H_{ex} can be derived based on the equations (1) and (2). Detail formulation was described in [9]–[10]. The excess heat can be written as a function of ΔT. Therefore, excess heat evaluation by the Ni bulk calibration curve shown in Fig. 3(b) is valid under the assumptions described in [9]–[10].

3.2. Excess Heat Generation

An Example of excess heat generation is shown in Fig. 6. The used samples were covered with 6 CuNi layers (Cu=2 nm and Ni=14 nm). The red and blue lines represent excess heat and pressure of the chamber, respectively. At the beginning of the experiment, hydrogen gas was introduced to the chamber up to 200Pa and absorbed into the Ni based nano-sized multilayer metal composite at about 270°C. The pressure for each experiment gradually decreased as shown in Fig. 6. The amount of hydrogen absorbed by each sample was estimated based on the pressure change and temperature of the chamber. After about 16 hours, H_2 gas was evacuated and simultaneously each sample was heated up by the ceramic heater. After that, heat energy greater than input power was observed. The input power was stable during one cycle; for example, 19 W was applied to the ceramic heater from about 6×10^4 sec to about 1×10^5 sec.

Released excess energy per hydrogen was evaluated based on the experimental result. The amount of absorbed hydrogen, total excess energy and excess energy per absorbed hydrogen are shown in Fig. 6. The amount of excess energy was calculated as 0.76 MJ by time integration of excess power. Although it seems highly unlikely that all the absorbed hydrogen atoms reacted, we can still estimate that average released energy per absorbed total hydrogen was 12 keV/H. In the previously reported example, a total of 1.1 MJ of energy was released, and the energy released per hydrogen was 16 keV/H [9], [10], [13]. Although the released energy is somewhat lower than that, it is still definitely not at a level that can be explained by chemical reactions.

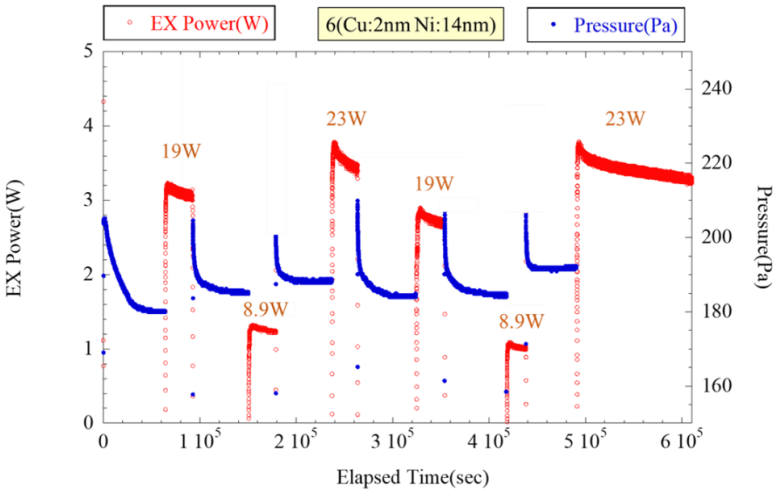

Absorbed H [mol]	6.7E-04
Absorbed Number of H	4.0E+20
Total Excess Energy [J]	7.6E+05
Excess Energy Density [J/H-mol]	1.1E+09
Excess Energy Density [eV/H]	1.2E+04

Figure 6. An example of excess heat generation

3.3. Heat Burst Phenomena

As the heat generation experiments proceeded, we began to observe a sudden increase in the amount of heat generated. In this section, we describe these heat burst phenomena, in which a rapid surface temperature increase is observed. First, examples of phenomena that cause spontaneous heat bursts are described, and then examples of intentional heat burst phenomena are described using a method devised based on observations of spontaneous heat bursts.

3.3.1. *Spontaneous Heat Burst*

Figure 7 shows an example of a spontaneous heat burst, in which temperature time variations of the temperatures for the thermocouple, surface A and B are plotted [9]–[10]. First, the temperature of surface A suddenly rises, and about 100 seconds later, the temperature of surface B rises. While these surface temperature increases are occurring, the temperature of the thermocouple embedded in the center of the heater is also gradually increasing. Detailed observations of the temperature change of the thermocouple shows that the temperature of the thermocouple increases 33 seconds after the temperature of surface A suddenly rises. Furthermore, the slope of the temperature rise of the thermocouple then increases 40 seconds after the temperature of surface B suddenly rises. From this we conclude that the heat release reaction occurred at the surface A at first and afterwards at the surface B, and heat bursts propagated to the thermocouple. Input power and room temperature were constant during these events. Therefore, these events were not caused by the change of electrical input power or heat coming in from the environment. The samples consisted of 6 layers of Cu (2 nm) and Ni (14 nm) fabricated by magnetron sputtering on Ni bulk, the same method as in [9]–[16].

Considering the material and thickness of the sample holder containing the heater, the delay time when heat is generated at the surface of the sample was roughly consistent with the observed delay time of 33 or 40 seconds [12]. Therefore, it is consistent with the interpretation that heat was generated at the sample surface and transferred to the thermocouple at the center.

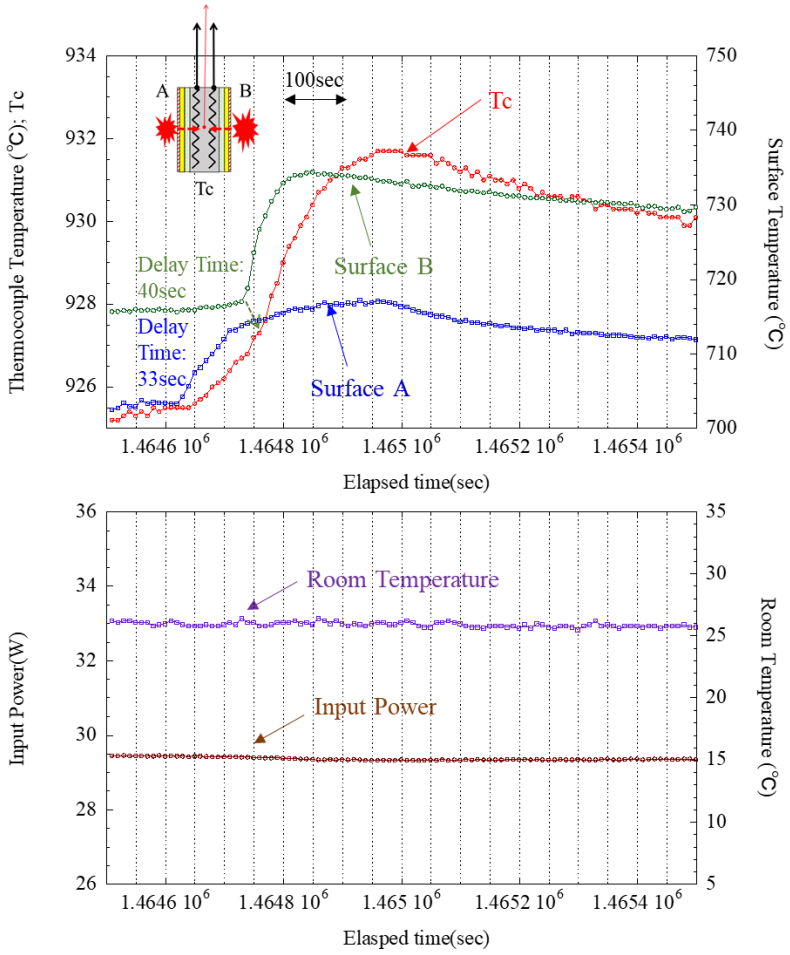

Figure 7. An example of spontaneous heat burst; Heat burst reactions occurred at surface A at first and afterwards at surface B. Their heat bursts propagated to the Tc. Input power and room temperature were constant during these events [12].

3.3.2. *Intentional Heat Burst*

When analyzing the phenomenon of spontaneous sudden heat bursts described above, it was observed that there were cases where the heat burst occurred after small changes in input power caused by fluctuations in the outside temperature, etc. Therefore, we tried to see if we could induce the heat burst by intentionally causing a small perturbation in the input power.

An example of a heat burst induced by an intentional perturbation of input electrical power is shown in Fig. 9(a). In this example, samples of 6 layers of Cu (2 nm) and Ni (14 nm) were fabricated by magnetron sputtering on Ni bulk. At the beginning, 25.8 W was input, and then decreased to 25.0 W. Then the T_C and surface temperature A and B decreased gradually. When the input was returned to the original input of 25.8 W, the surface temperature A, B, and T_c all increased and became larger than the values at the original input of 25.8 W. At maximum, T_c increased by about

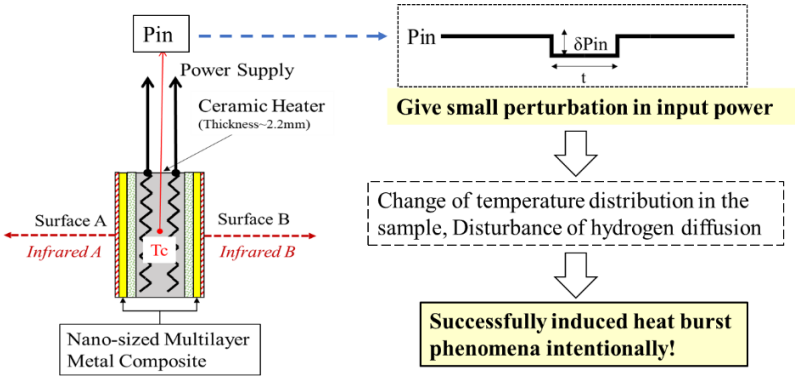

Figure 8. Intentional induction of heat burst phenomena.

9°C, surface A by about 17°C, and surface B by about 25°C. The increases in surface A and B temperatures were larger and steeper than that of T_c as shown in Fig. 9(a). We conclude that heat burst energy generated at the surface A and B, which is induced by the intentional perturbation of input power, propagated to the thermocouple.

On the other hand, an example with no heat burst phenomenon induced by a similar perturbation is shown in Fig. 9(b). In this case, Ni bulk samples were used. When the input power, which was initially 23.0 W, was reduced to 22.1 W, the thermocouple and surface temperatures A and B gradually decreased. Then, when the input power was returned to 23.0 W, the heat burst phenomenon did not occur, and the thermocouple and surface temperatures A and B returned to their original values.

Next, we examine the possibility that the observed heat burst phenomenon was caused by some chemical reactions. Figure 10 plots the change in Tc during the heat burst shown in Fig. 9(a). A heat burst induced by perturbation of input power lasted for at least 1.2×10^4 seconds. The amount of generated energy is more than the hatched region in Fig. 10. The first time in this hatched triangle corresponded to 6.0 W of excess heat, and the last time to finish the experiment was 5.6 W of excess heat. Therefore, the hatched triangle can be calculated as 5.6 to 6.0 W $\times$ 1.2E4 s = 4.8 kJ. Therefore, energy generated by a single intentionally induced heat burst is more than 4.8 kJ in this example.

Consider the following chemical reactions that may cause a heat burst:

(1) If all the residual gas is oxygen and the absorbed hydrogen is oxidized and generates heat.
(2) If the residual gas is oxygen, and the Ni metal is oxidized by it.
(3) If the residual gas consists of mixed gas (H_2:O_2=2:1), the combustion energy would give energy to the surface of the two samples.

During the heat release experimental cycle, all the hydrogen introduced for absorption was evacuated, and the degree of vacuum was less than 1×10^{-4} Pa when the heat burst phenomenon was observed. The volume of the chamber is about 9 L, so the number of moles of residual gas was less than 4×10^{-10} mol. It is known that the combustion reaction of hydrogen is about 290 kJ/mol and the heat of formation of nickel oxide is about 240 kJ/mol. Based on the number of moles of residual gas in the chamber, the heat generated in each case can be calculated as less than (1) 6×10^{-5} J, (2) 2×10^{-4} J and (3) 8×10^{-5} J. Comparing these values to the energy increased by the heat burst, 4.8 kJ, shows that they are completely negligible. This clearly shows that at least the chemical reactions (1)-(3) cannot explain the heat burst phenomenon observed in this study. Therefore, the amount of energy generated by a single intentionally induced heat burst cannot be explained by any known chemical reaction.

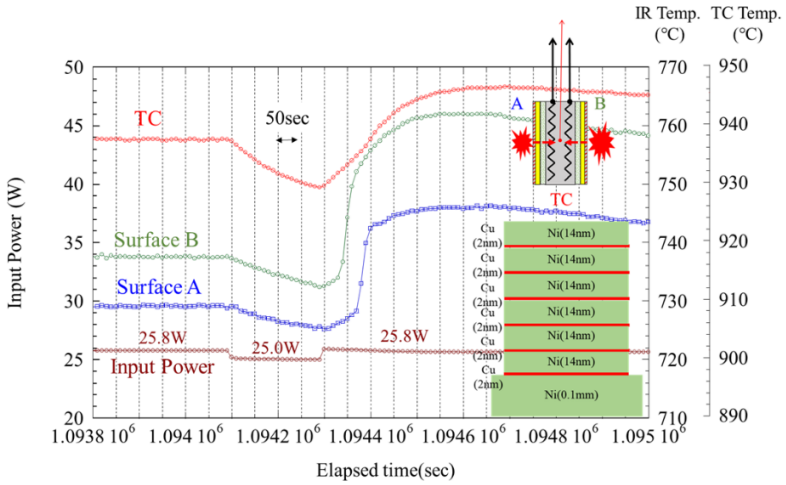

(a)

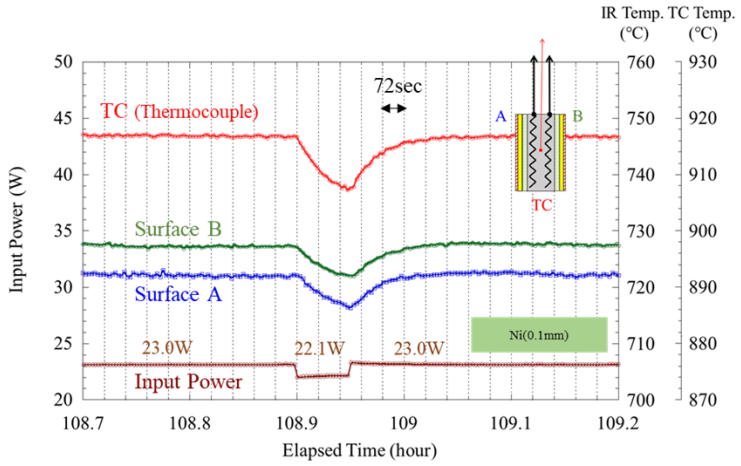

(b)

Figure 9. Different responses to intentional perturbations of input power: (a)An example of heat burst phenomenon induced by an intentional perturbation of input electrical power using CuNi multilayer samples, (b) An example where no heat burst phenomenon was induced by a similar perturbation using Ni bulk samples.

Next, we show how the intentional heat burst varies greatly, depending on sample composition and other factors. Figure 11(a) shows an example of heat burst for a 6-layer CuNi(CaO) sample with a 4.5 nm CaO layer inserted in a 14 nm Ni layer. Similar to the previous CuNi example (Fig. 9(a)), the heat burst phenomenon occurs after about 60 seconds for surface B and 120 seconds for surface A, respectively, after the input power is returned to its original value. Generated heat propagates to the heater center and the thermocouple temperature increases, similar to Figure 9(a). This type of heat burst is the most common among the experiments conducted so far.

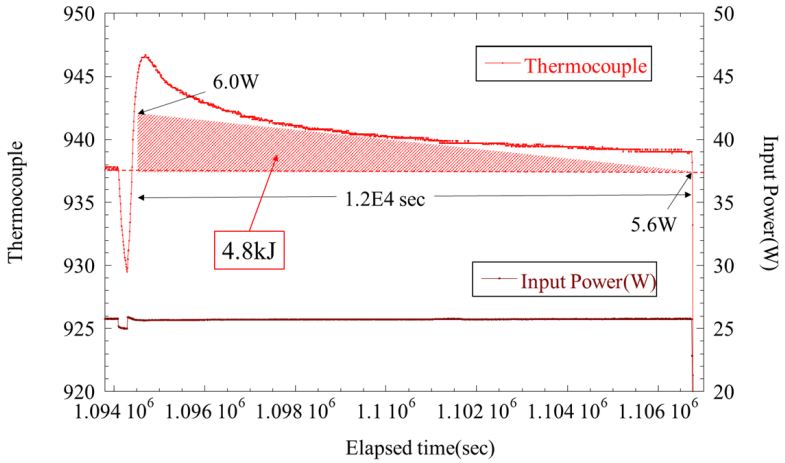

Figure 10. The amount of energy generated by an intentionally induced heat burst.

Table 1. Mill sheet for Ni bulk.

Element	Concentration (weight %)
Si	0.26
C	0.10
Mn	0.01
Mg	0.03

Figure 11(b) shows an example of a different type of intentional heat burst. After the input power was reduced from 28.4 W to 27.5 W, the heat burst phenomenon occurred on surface B before the power was increased back to 28.4 W. A weak heat burst phenomenon appears to have occurred on surface A at about the same time. Also, as before, after the input power was returned to 28.4 W, the heat burst phenomenon occurred again about 80 seconds later on surface A and about 130 seconds later on surface B. Note that the Cu thickness of this sample is thicker than usual, and the ratio of Cu to Ni is about 4.3.

It is possible to qualitatively induce this intentional heat burst phenomenon with high reproducibility in $CuNi_7$ samples of standard composition. From previous experiments, it is also known that this heat burst phenomenon depends on (1) the composition and structure of the sample, (2) the surface temperature of the sample, and (3) the magnitude and time width of the perturbation of the input power. In the experiments we are currently conducting, we are observing this heat burst phenomenon under various parameters, and we are attempting to elucidate the mechanism of the phenomenon.

3.4. Material Analysis

Various analytical methods have been applied to clarify the mechanism of the heat generation phenomenon in nano-sized multilayer metal composites. In this section, we describe the results of SEM-EDX (Scanning Electron Microscope - Energy Dispersive X-ray Spectroscopy) and TOF-SIMS (Time-Of-Flight Secondary Ion Mass Spectrometry) and discuss the obtained results.

Table 1 shows the mill sheet of the Ni bulk used for the experiments. The main impurities are Si, C, Mn and Mg. The impurities vary a little with the batch of Ni bulk, but the main impurities in Ni material are Si and Mn.

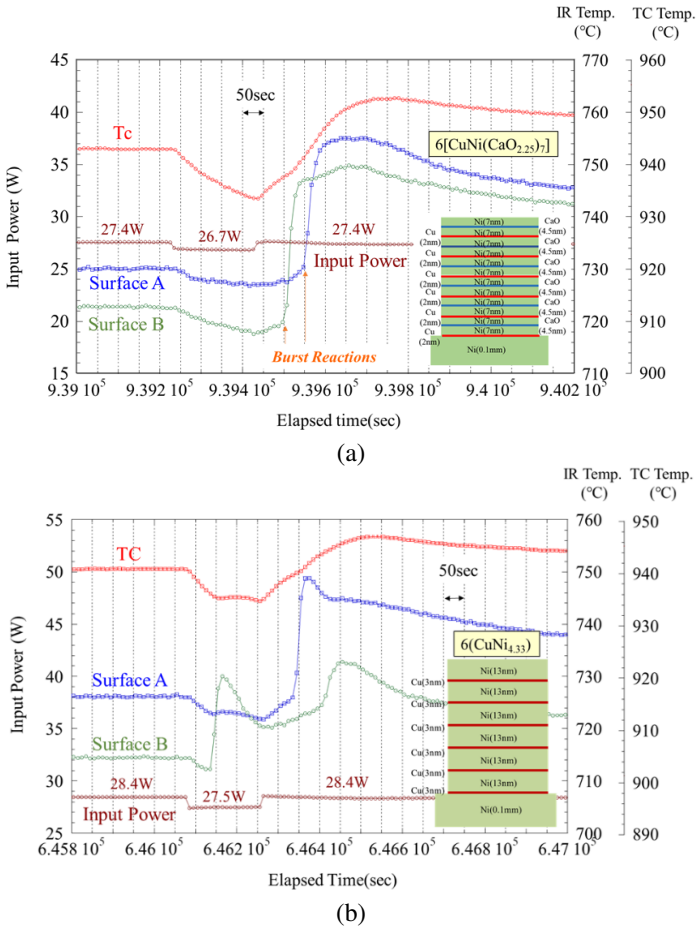

Figure 11. Variation of heat burst phenomena triggered by input power perturbation.

We normally perform SEM and EDX analysis of the sample surface for each experiment. The results of these analyses have revealed some common characteristics of the samples which produce excess heat. One example is shown in Figure 12. On the left side are the secondary electron images, and the right side are the compositional images (COMPO images) by backscattered electrons. It shows the presence of Ni crystal grains and grain boundaries ranging from several 10 μm to 100 μm. Characteristic is the presence of spotted parts in both images, which appear to be composed of elements lighter than Ni. As will be mentioned later, these black spots are areas of very high oxygen concentration.

Figure 13 shows the SEM-EDX analysis for the spontaneous heat burst sample shown in Fig. 7. Figures 13(a) and 13(b) are black spot areas, where a distinct oxygen peak is detected in the EDX spectrum, indicating a high atomic number ratio of 18% to 21%. On the other hand, Figure 13(c) is a normal area, indicating that oxygen is below the detection limit.

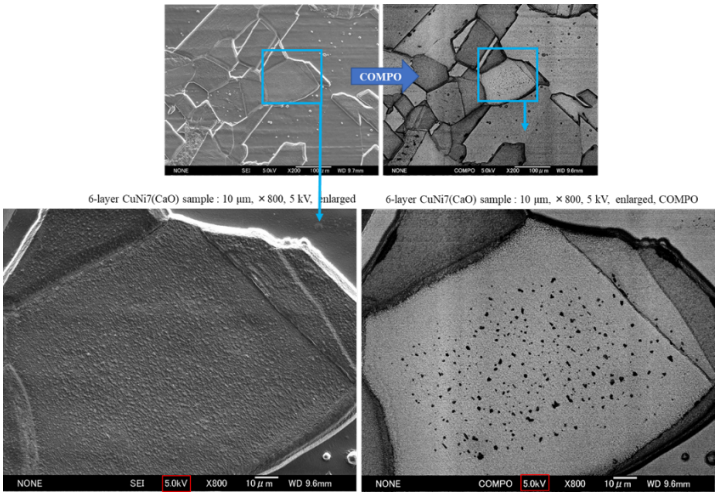

Figure 12. An example of SEM analysis after heating experiment. The spotted regions within the grains can be observed, which seems to be common to samples that observed excess heat.

Because the samples were exposed to the atmosphere after the experiment, they should be covered with NiO, however, the NiO layer is so thin that it is usually below the detection limit in the EDX spectrum, less than 1% by atomic number. Also, the Cu deposited before the experiment is not detected in the EDX spectrum because the deposited Cu was very thin, and the Cu diffused into the interior during the experiment.

Figure 14 shows SEM-EDX & TOF-SIMS analyses of the intentional heat burst sample shown in Figure 11(a). Figure 14(a) shows the result after an experiment using a sample of 6-layer CuNi7 (Cu=2nm, Ni=14nm) with 4.5nm of CaO inserted in the Ni layer: intentional heat burst phenomenon occurred. In the normal area on the left side of the figure, only Ni is detected, but in the black spot area on the right side, nearly 33% oxygen is detected by EDX.

Figure 14(b) shows the depth profile by TOF-SIMS analysis for areas with abundant black spots. Since TOF-SIMS has a larger beam diameter than EDX, we selected a region in this sample with relatively many black spots for analysis. This data is obtained using negative ion (Cs^-) and ion energy was 2 kV and ion current was 40 nA. In this TOF-SIMS analysis, the vertical axis represents the dimensionless number of counts for each ion divided by the total number of counts. As can be seen in this graph, the most abundant ion is O−, with a value of nearly 40%. Note that the orange vertical dashed line in the figure for each ion indicates the area near the interface between the surface multilayer and the Ni bulk. Although the TOF-SIMS signal is difficult to discuss quantitatively because the values vary depending on the ionizability of each element, there is no doubt that the oxygen concentration is high not only on the surface of the sample but also in the interior of the sample. Thus, for the sample in which the intentional heat burst was observed, there were spots of very high oxygen concentration by SEM-EDX, and TOF-SIMS analysis also supported the results.

An experiment was conducted to see if a black spot area of very high oxygen concentration, which was frequently observed in heat-producing samples, was caused by exposing oxygen in the air after the experiment. Figure 15 shows a selection of the highest oxygen concentration areas in the analysis results of a sample that was once removed from the chamber during the experiment, forced to oxidize at 500°C for 2 hours under atmospheric pressure, returned to the chamber, and then hydrogenated and heated again. No black spots with very high oxygen concentration were observed in this sample; Ni, Cu, Mn, Si, O, and C were observed at the grain boundary and at points 29–31, suggesting that Mn and Si are impurities in the Ni bulk and C is derived from hydrocarbons in the air. Cu, which had not been

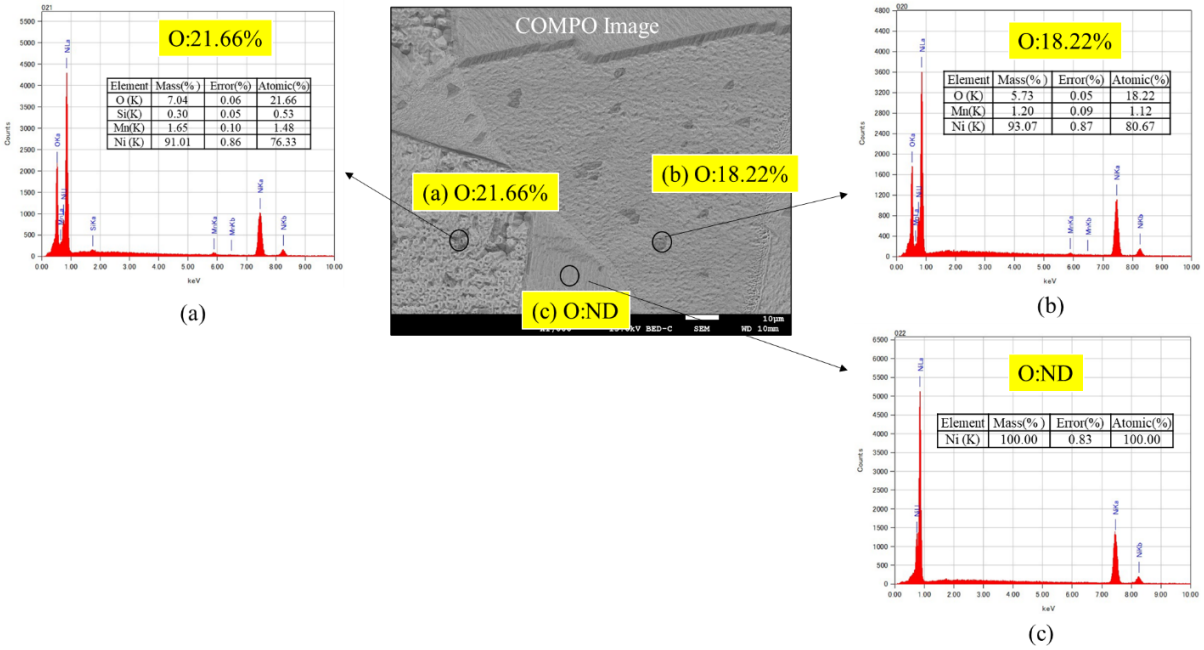

Figure 13. SEM-EDX analysis for the spontaneous heat burst sample shown in Fig. 7: (a) black spot area, (b) another black spot area, (c) normal area.

observed by EDX before, was observed in this sample. The oxygen concentration was a maximum of 4–5% at grain boundaries (31 points) and 2–3% at other points. The emissivity measured after treatment at 500°C under atmospheric pressure was almost 1, indicating that the surface was covered with a thick oxide film. Thus, once the sample has undergone forced surface oxidation, the oxygen concentration is less than 5%, even though it is mostly reduced due to the hydrogen absorption process and subsequently exposed to the atmosphere. The large number and frequency of regions with oxygen concentrations exceeding 10%, as shown in Figures 13 and 14, is an anomaly.

3.4.1. *Discussion*

In this paper, the heat burst phenomenon was described. The research implications of heat bursts are as follows. Excess heat generation is evaluated using a calibration curve. The reader may wonder whether the heat dissipation conditions are different between the time of calibration and the time of the heat generation experiment due to variations in the way the sample is mounted, etc. This is a reasonable question. However, since the heat burst phenomena were observed under the same heat dissipation conditions, it cannot be explained by the difference in heat dissipation conditions between the calibration and heat generation experiments. Therefore, it can be said that observing heat burst phenomena enhances the reliability of excess heat experiments.

The experimental results related to heat burst phenomenon were observed by the Focardi team [18]. They used Ni rods and hydrogen. They observed excess heat by once bringing the temperature of the Ni rods down to near room temperature and then abruptly returning them to their original input power level. Although the experimental

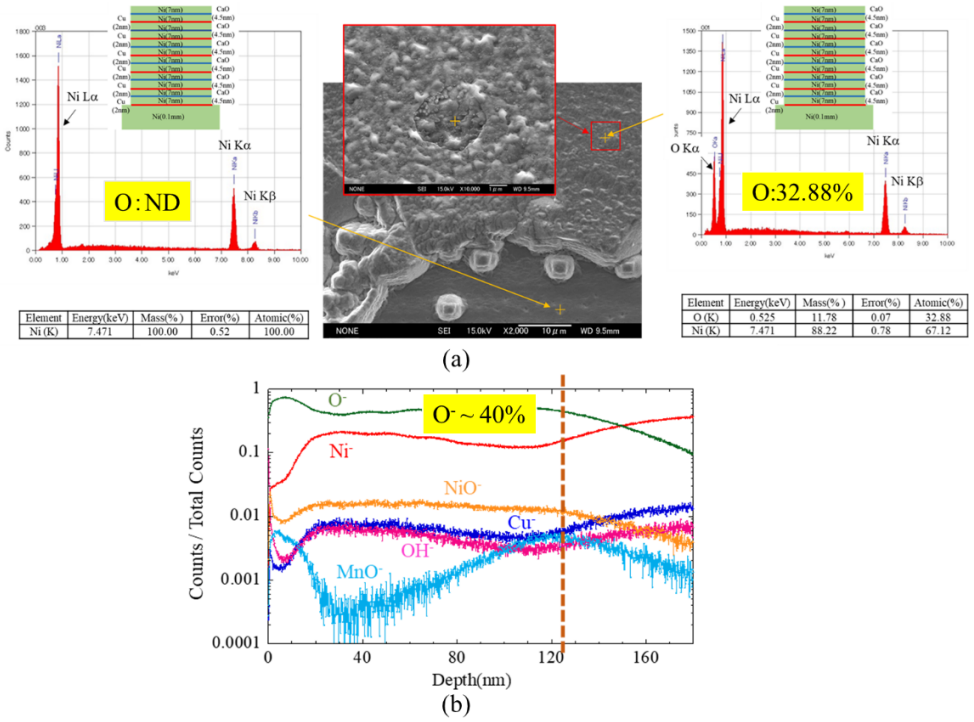

Figure 14. SEM-EDX & TOF-SIMS analysis of the intentional heat burst sample shown in Figure 11(a): (a) SEM-EDX analysis results for normal and black spot areas; (b) TOF-SIMS analysis results for areas with abundant black spots.

methods are different, the same physicochemical mechanism related to the diffusion of hydrogen seems to be behind the experimental results.

Why were these described phenomena observed in CuNi multilayers? At present, we do not have a clear answer to this question. However, the NEDO project observed anomalous heating in Cu and Ni powders [6]–[8], and Celani et al. observed anomalous heating in constantan wire, an alloy of Cu and Ni [19]. Our experiments on heat generation in multilayers of CuNi were inspired by these results.

We are currently attempting to explain the phenomenon by a trapping hydrogen hypothesis as shown in Fig. 16. The hydrogen is absorbed in the bulk Ni and in the Ni/Cu mixed layer, and then the hydrogen inside diffuses by evacuation and rapid heating by the heater. Many hydrogen atoms can be trapped in the trapping sites, such as vacancy, dislocation, or voids. The perturbation of the input power causes a fluctuation in hydrogen density, which might trigger the heat burst phenomena.

4. Concluding Remarks

An innovative method to induce anomalously large heat generation phenomena that cannot be explained by known chemical processes has been developed. Ni-based nano-sized multilayer film was preloaded with hydrogen gas and heated rapidly to diffuse hydrogen and induce a heat generation reaction. Not only steady-state anomalous heat generation, but also spontaneous heat bursts were sometimes observed. Based on the observation of spontaneous heat

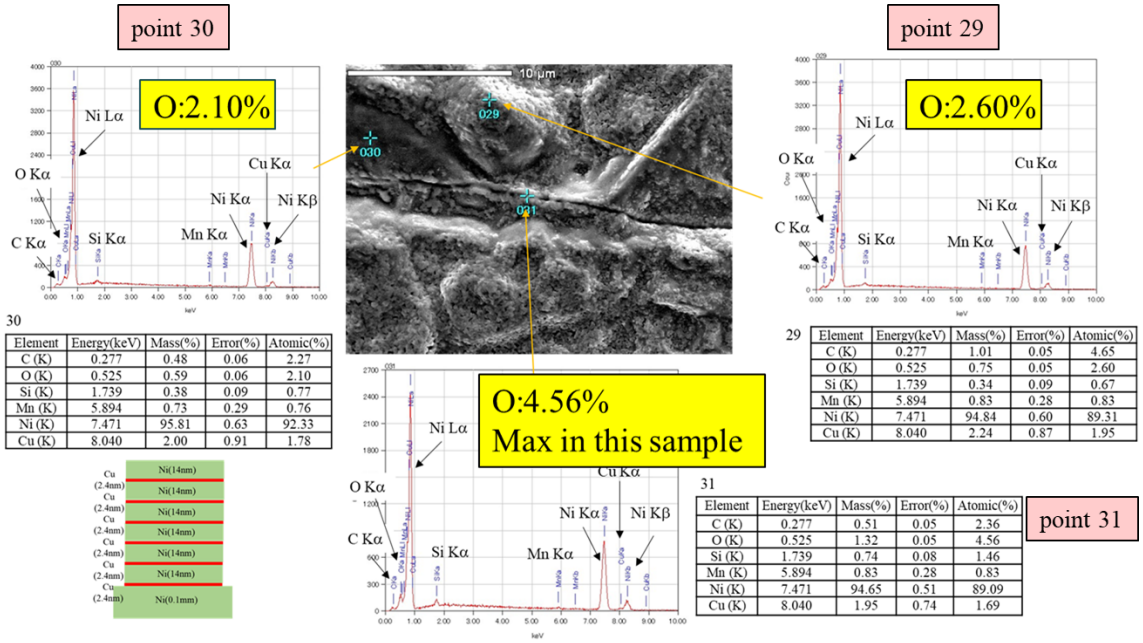

30

Element	Energy(keV)	Mass(%)	Error(%)	Atomic(%)
C (K)	0.277	0.48	0.06	2.27
O (K)	0.525	0.59	0.06	2.10
Si (K)	1.739	0.38	0.09	0.77
Mn (K)	5.894	0.73	0.29	0.76
Ni (K)	7.471	95.81	0.63	92.33
Cu (K)	8.040	2.00	0.91	1.78

29

Element	Energy(keV)	Mass(%)	Error(%)	Atomic(%)
C (K)	0.277	1.01	0.05	4.65
O (K)	0.525	0.75	0.05	2.60
Si (K)	1.739	0.34	0.09	0.67
Mn (K)	5.894	0.83	0.28	0.83
Ni (K)	7.471	94.84	0.60	89.31
Cu (K)	8.040	2.24	0.87	1.95

31

Element	Energy(keV)	Mass(%)	Error(%)	Atomic(%)
C (K)	0.277	0.51	0.05	2.36
O (K)	0.525	1.32	0.05	4.56
Si (K)	1.739	0.74	0.08	1.46
Mn (K)	5.894	0.83	0.28	0.83
Ni (K)	7.471	94.65	0.51	89.09
Cu (K)	8.040	1.95	0.74	1.69

Figure 15. SEM-EDX Analysis for the forced oxidated sample: This sample was taken out and oxidized at 500°C for 2 hours in the air. After that normal experimental process was performed.

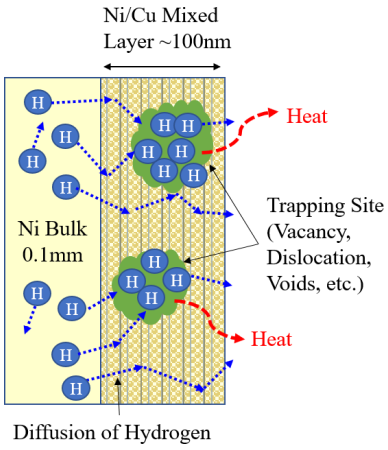

Figure 16. Trapping hydrogen hypothesis.

bursts, intentional heat bursts have also become possible. Even a single heat burst phenomenon cannot be explained by any known chemical reactions. Observation of heat bursts has improved the reliability of the excess heat experiments. Samples that generated excess heat or heat bursts often show some areas of very high oxygen concentration (higher than

in a forced oxidized sample) after the experiment according to SEM-EDX and TOF-SIMS analyses. The reason for this is currently unknown, and we would like to investigate the mechanism by assuming a trapped hydrogen hypothesis.

Acknowledgements

The authors would like to thank President H. Yoshino and all the members of CLEAN PLANET Inc. for their significant contribution. The authors also thank Mr. Y. Shibasaki and Prof. H. Kikunaga for their support. This work is supported by the Research Center for Electron Photon Science of Tohoku University, CLEAN PLANET Inc., The Thermal & Electric Energy Technology Foundation, the Iwatani Naoji Foundation and the Tanaka Kikinzoku Memorial Foundation.

References

[1] Y. Iwamura, M. Sakano and T. Itoh, "Elemental Analysis of Pd Complexes: Effects of D_2 Gas Permeation", *Japanese Journal of Applied Physics*, **41** (2002) 4642-4650.

[2] Y. Iwamura et. al, "Observation of Low Energy Nuclear Transmutation Reactions Induced by Deuterium Permeation through Multilayer Pd and CaO thin Film", *J. Condensed Matter Nucl. Sci.* **4** (2011) 132–144.

[3] Y. Iwamura, T. Itoh and S. Tsuruga, "Transmutation Reactions Induced by Deuterium Permeation through Nano-structured Pd Multilayer Thin Film", *Current Science,* **108** (2015) 628-632.

[4] Y. Iwamura, "Review of permeation-induced nuclear transmutation reactions", *Cold Fusion: Advances in Condensed Matter Nuclear Science*, Ed. Jean-Paul Biberian, Elsevier, Amsterdam, (2020)191-204.

[5] Tatsumi Hioki et al, Inductively Coupled Plasma Mass Spectrometry Study on the Increase in the Amount of Pr Atoms for Cs-Ion-Implanted Pd/CaO Multilayer Complex with Deuterium Permeation, *Jpn. J. Appl. Phys*. **52** (2013)107301.

[6] Y. Iwamura, T. Itoh, J. Kasagi, A. Kitamura, A. Takahashi and K. Takahashi, "Replication Experiments at Tohoku University on Anomalous Heat Generation Using Nickel-Based Binary Nanocomposites and Hydrogen Isotope Gas", *J. Condensed Matter Nucl. Sci.* **24** (2017) 191–201.

[7] Y. Iwamura, T. Itoh, J. Kasagi, A. Kitamura, A. Takahashi, K. Takahashi, R. Seto, T. Hatano, T. Hioki, T. Motohiro, M. Nakamura, M. Uchimura, H. Takahashi, S. Sumitomo, Y. Furuyama. M. Kishida and H. Matsune, "Anomalous Heat Effects Induced by Metal Nano-composites and Hydrogen Gas", *J. Condensed Matter Nucl. Sci.* **29** (2019) 119–128.

[8] A. Kitamura, A. Takahashi, K. Takahashi, R. Seto, T. Hatano, Y. Iwamura, T. Itoh, J. Kasagi, M. Nakamura, M. Uchimura, H. Takahashi, S. Sumitomo, T. Hioki, T. Motohiro, Y. Furuyama, M. Kishida, H. Matsune, "Excess heat evolution from nanocomposite samples under exposure to hydrogen isotope gases", *International Journal of Hydrogen Energy* **43** (2018) 16187-16200.

[9] Y. Iwamura, J. Kasagi, T. Itoh, T. Takahashi, M. Saito, Y. Shibasaki and S. Murakami, "Progress in Energy Generation Research using Nano-Metal with Hydrogen/Deuterium Gas", *J. Condensed Matter Nucl. Sci.* **35** (2022) 285–301.

[10] Y. Iwamura, T. Itoh, T. Takahashi, S. Yamauchi, M. Saito, S. Murakami and J. Kasagi, "Energy Generation using Nano-sized Multilayer Metal Composites with Hydrogen Gas; Intentional Induction of Heat Burst Phenomenon", *Proceedings of the 22nd Meeting of Japan CF Research Society*, JCF22, March 5, 2022, Online Meeting, p.27-39.

[11] T. Itoh, S. Shibasaki, T. Takahashi, M. Saito, J. Kasagi and Y. Iwamura, "Optical Observation on Anomalous Heat Generation from Nano-sized Metal Composite", *J. Condensed Matter Nucl. Sci.* **35** (2022) 274–284.

[12] Y. Iwamura, T. Itoh, M. Saito, S. Murakami and J. Kasagi, "Evidence for Surface Heat Release Reaction over Nano-sized Multilayer Metal Composite with Hydrogen Gas", *Proceedings of the 21st Meeting of Japan CF Research Society*, JCF21, December 11-12, 2020, Online Meeting, pp. 1–14.

[13] Y. Iwamura, T. Itoh, J. Kasagi, S. Murakami and M. Saito, "Excess Energy Generation using a Nano-sized Multilayer Metal Composite and Hydrogen Gas", *J. Condensed Matter Nucl. Sci.* **33** (2020) 1–13.

[14] T. Itoh, S. Shibasaki, J. Kasagi, S. Murakami, M. Saito and Y. Iwamura, "Optical Observation on Anomalous Heat Generation from Nano-sized Metal Composite", *Proceedings of the 21st Meeting of Japan CF Research Society*, JCF21, December 11-12, 2020, Online Meeting, pp. 15–25.

[15] M. Saito, T. Itoh, Y. Iwamura, S. Murakami and J. Kasagi, "Elemental Analysis for Elucidation of the Anomalous Heat Generation Phenomena", Proceedings of the 20th Meeting of Japan CF Research Society, JCF20, December 13-14, 2019, Reference Hakata Eki-Higashi Rental Room, Fukuoka, Japan pp. 74–85.
[16] S. Murakami, T. Itoh, Y. Iwamura, M. Saito and J. Kasagi, "Excess Energy Generation Experiments using a Nano-sized Multilayer Metal Composite and Hydrogen Gas", Proceedings of the 20th Meeting of Japan CF Research Society, JCF20, December 13-14, 2019, Reference Hakata Eki-Higashi Rental Room, Fukuoka, Japan pp. 86–96.
[17] Y. Fukai, Evidence for Quantum Diffusion of Hydrogen in Ta: Quench-Recovery Experiments Revisited, *Japanese Journal of Applied Physics*, Vol.23, No.8 (1984) 596–598.
[18] S. Focardi, V. Gabbani, V. Montalbano, F. Piantelli and S. Veronesi, Large excess heat production in Ni-H systems, *Il Nuovo Cimento A (1971–1996)* **111** (1998) 1233–1242.
[19] F. Celani et al., "Cu–Ni–Mn alloy wires with improved sub-micrometric surfaces used as LENR device by new transparent dissipation-type calorimeter", *Journal of Condensed Matter Nuclear Science* **13** (2014) 56–67.